Resonance Raman spectroscopy in Si and C ion-implanted double-wall carbon nanotubes

G. D. Saraiva,[1] A. G. Souza Filho,[2,*] G. Braunstein,[3] E. B. Barros,[2] J. Mendes Filho,[2] E. C. Moreira,[4] S. B. Fagan,[5] D. L. Baptista,[6] Y. A. Kim,[7] H. Muramatsu,[7] M. Endo,[7] and M. S. Dresselhaus[8]

[1]*Universidade Estadual do Ceará, 60740-000 Fortaleza, CE, Brazil*

[2]*Departamento de Física, Universidade Federal do Ceará, Caixa Postal 6030, CEP 60455-900 Fortaleza, CE, Brazil*

[3]*Micron Technology Inc., 9600 Godwin Drive, Manassas, Virginia 20110, USA*

[4]*Universidade Federal do Pampa (UNIPAMPA), Campus Bagé, 96412-420 Bagé, RS, Brazil*

[5]*Centro Universitário Franciscano–UNIFRA, 97010-032 Santa Maria, RS, Brazil*

[6]*Departamento de Física, Universidade Federal do Rio Grande do Sul, 91501-970 Porto Alegre, RS, Brazil*

[7]*Faculty of Engineering, Shinshu University, 4-17-1 Wakasato, Nagano-shi 380-8553, Japan*

[8]*Department of Physics and Department of Electrical Engineering and Computer Science, Massachusetts Institute of Technology, Cambridge, Massachusetts 02139-4307, USA*

(Received 30 June 2009; revised manuscript received 5 September 2009; published 28 October 2009)

The effect of 170 keV Si and 100 keV C ion bombardment on the structure and properties of highly pure, double-wall carbon nanotubes has been investigated using resonance Raman spectroscopy. The implantations were performed at room temperature with ion doses ranging between 1×10^{13} ions/cm^2 and 1×10^{15} ions/cm^2. As expected, the Si irradiation created more disorder than the C irradiation for the same ion fluence. For both species, as the ion-implantation fluence increased, the *D*-band intensity increased, while the *G*-band intensity decreased, indicating increased lattice disorder, in analogous form to other forms of graphite and other nanotube types. The frequency of the *G* band decreased with increasing dose, reflecting a softening of the phonon mode due to lattice defects. With increasing ion fluence, the radial breathing modes (RBMs) of the outer tubes (either semiconducting or metallic) disappeared before the respective RBM bands from the inner tubes, suggesting that the outer nanotubes are more affected than the inner nanotubes by the ion irradiation. After Si ion bombardment to a dose of 1×10^{15} ions/cm^2, the Raman spectrum resembled that of highly disordered graphite, indicating that the lattice structures of the inner and outer nanotubes were almost completely destroyed. However, laser annealing partially restored the crystalline structure of the nanotubes, as evidenced by the re-emergence of the *G* and RBM bands and the significant attenuation of the *D* band in the Raman spectrum.

DOI: 10.1103/PhysRevB.80.155452 PACS number(s): 73.22.−f, 78.30.Na

I. INTRODUCTION

Carbon nanotubes have received much attention because of their unique physical properties and their promising potential for technological applications in optics, electronics, and in high-performance composites.[1] When used in applications such as nuclear reactors and space aircraft,[2] carbon nanotube-based composites will be exposed to energetic particle beams. The study of ion-beam irradiation effects on the structural and electronic properties of carbon nanotubes can help develop a better understanding of nanotube structural instabilities and can also shed light on the mechanisms behind the formation and dynamics of defects in carbon nanostructures, leading to more robust composites. In addition, irradiation of nanotubes with either electron or ion beams can be used to tailor structural modifications such as straining, bending, or breaking the tubes.

Radiation effects can induce different kinds of defects in carbon nanotubes, such as substitutional, interstitial, single, and multiple vacancies, which in turn are responsible for modifying the electronic, mechanical, optical, and chemical properties to a great extent. Indeed, ion beams have been successfully used for the nanoengineering of carbon nanostructures.[3] Striking phenomena, such as irradiation-assisted self-assembly, and self-organization have been reported. Band gap tailoring and carbon nanotube interconnects have been achieved using charged particle beams as well.[4–7] Furthermore, it appears that it is possible to modify their physical properties by changing their structure locally only along a short section of the tube.[8]

Most of the works devoted to study the effects of electron or ion-beam irradiation have involved single-walled and multiwalled carbon nanotubes. Pregler *et al.* reported Ar irradiation on nanotubes-polystyrene composites and found that double-wall carbon nanotubes (DWNTs)-based composites have significantly more crosslinks between nanotubes and a polymer matrix than for single wall carbon nanotubes (SWNTs)-based composites.[9] Here, we focus on the effects of Si and C ion bombardment on the structural properties of DWNTs. These systems can be viewed as the simplest form of multiwall carbon nanotubes (MWNTs) since DWNTs contain two coaxial SWNTs coupled to one another by van der Waals interactions. In DWNTs, the inner wall is somewhat isolated from the environment by an outer wall that might help preserve the intrinsic properties of the inner wall.

Resonance Raman spectroscopy is a noncontact and nondestructive characterization tool that probes the structural and electronic properties of carbon nanotubes and it is able to provide detailed information at the atomic scale. The strong and selective resonant process allows for the investigation of both semiconducting and metallic tubes. Furthermore, in the case of DWNTs, it is possible to probe the different outer or inner tube configurations and to analyze the

modifications on each tube shell separately.[10] The resonance Raman spectra of carbon nanotubes exhibit several characteristic spectral signatures. The most noteworthy, for the purposes of the present study, are (a) the first-order G band which is the nanotube version of the optical phonon mode of graphite, (b) the first-order radial breathing modes (RBMs), unique to nanotubes, which correspond to a coherent vibration of the carbon atoms in a direction perpendicular to the tube axis, (c) the second-order disorder-induced D band, which is also observed in disordered graphite, and (d) the G' band which is the second harmonic of the D band.[11] As defects are introduced in the nanotube structure, these characteristic Raman bands change in intensity, energy, and line shape. Significant understanding of the microstructural evolution of the irradiated samples can be gained by monitoring the evolution of these bands upon ion bombardment.

In this work, we report on the effects of Si and C ion irradiations on highly pure DWNTs (free of catalysts, amorphous carbon, and SWNTs) using resonance Raman spectroscopy as a characterization tool. We observe that as the ion dose increases, the G-band frequency and intensity decrease, the D-band intensity increases, and the RBMs disappear. The RBMs of the outer tubes disappear before the RBM for the inner tubes. For a Si ion-implantation dose of 1×10^{15} ions/cm^2, the Raman spectrum is typical of highly disordered graphite. However the G and RBM bands reemerge in Raman spectra taken after subsequent laser annealing. These changes in the Raman spectra of ion irradiated DWNTs are discussed in terms of the evolution of the lattice disorder induced by the bombarding ions.

II. EXPERIMENTAL DETAILS

The DWNTs studied in this work were produced by a catalytic chemical vapor deposition (CCVD) method, utilizing a conditioning catalyst (Mo/Al_2O_3), and a nanotube growth catalyst (Fe/MgO). The CCVD method for preparing the DWNTs has been described in detail elsewhere.[12] Generally, a two-step purification process is applied to the synthesized products whereby the DWNTs are treated by hydrochloric acid with 18% concentration, at 100 °C, for 10 h, in order to remove the MgO and iron catalyst particles. Using this approach, a black DWNT bucky paper sample was obtained which was thin, flexible, and tough enough mechanically to fold in origami.[12] The inset to Fig. 1 shows a scanning electron microscope image of the sample. Magnetic characterization of this DWNT bucky paper revealed a diamagnetic behavior, thus confirming the absence of magnetic metallic catalyst particles dispersed within the DWNT bundles.[12]

The DWNT bucky paper sample (highly purified with less than 1% of SWNTs and catalyst particles) and 0.1 mm thick was divided into small pieces and each piece was subsequently implanted with 170 keV Si or 100 keV C ions using doses ranging from 1×10^{13} to 1×10^{15} ions/cm^2. The Raman spectra were recorded with a Jobin Yvon T64000 spectrometer, equipped with a N_2-cooled charge coupled device (CCD) detection system. The 514.5 nm (green line −2.41 eV) and 488.0 nm (blue line −2.54 eV) lines of an argon ion laser were used for excitation of the Raman spectra. An Olympus microscope lens with a focal distance $f=20.5$ mm and a numerical aperture NA=0.35 was used to focus the laser on the sample surface. The laser beam diameter on the sample surface is about 0.7 μm. The laser power was about 1 mW impinging on the sample surface. By considering the skin depth of graphite, it is likely that the laser penetration on the sample is about 500 nm. Therefore, this technique mainly probes the tubes near the surface. The measured spectral lines had a resolution of 2 cm^{-1}. The Raman measurements were performed on the ion-irradiated side of the bucky paper because it was too thick to be transparent to the ion beams. Measurements on the back side of the samples indicated that the tubes were not modified, except for the highest ion dose, for which we observed only a slight change in the intensity of the overall Raman spectrum.

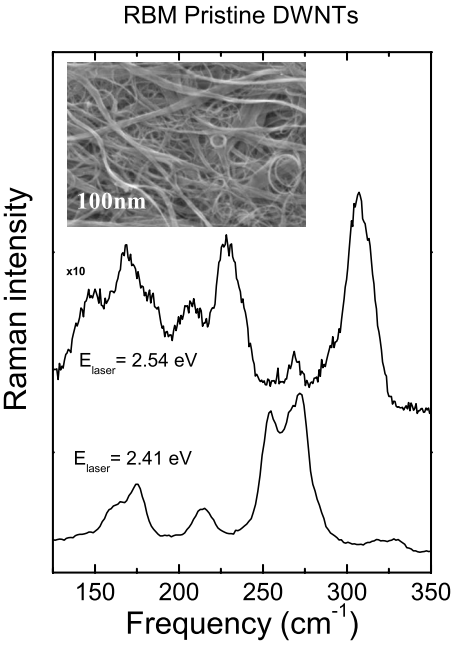

FIG. 1. RBM Raman spectra of pristine DWNTs obtained with two different laser lines, as indicated. The inset shows a scanning electronic image of the DWNT bundles used for ion implantation.

III. EXPERIMENTAL RESULTS

A. Pristine samples

In order to analyze the effect of ion implantation on the DWNT samples, we first present the Raman spectra of pristine samples (nonirradiated) and identify the nanotube categories which are contributing to the resonance Raman spectra. Figure 1 shows the Raman spectra, in the RBM mode region, for nonirradiated samples, taken with two different laser lines (E_{laser}=2.54 and 2.41 eV). These laser energies probe the $M@S$ and $S@S$ (inner@outer; M and S denote metallic and semiconducting, respectively). Here, we see that the pristine DWNT sample exhibits radial breathing mode Raman spectra from the inner tubes (higher frequency) and outer tubes (lower frequency). In bundle samples, such as those used in the present study, it is not possible to assure

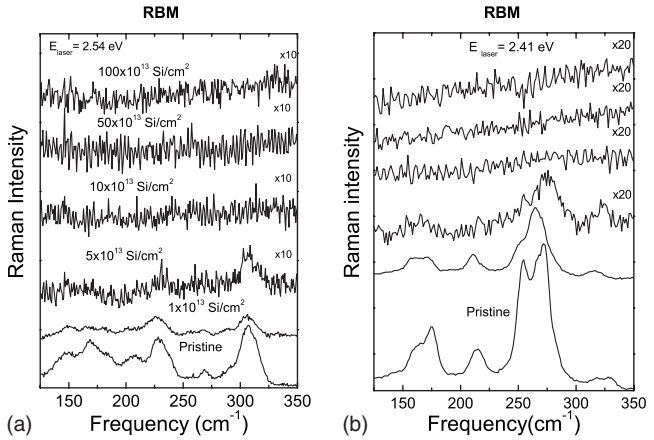

FIG. 2. RBM Raman spectra of Si^+ bombarded DWNT samples for two different laser excitation energies, (a) 2.54 eV and (b) 2.41 eV, and for different 170 keV Si^+ ion fluences. The same sample set was used for the data taken at the two laser energies.

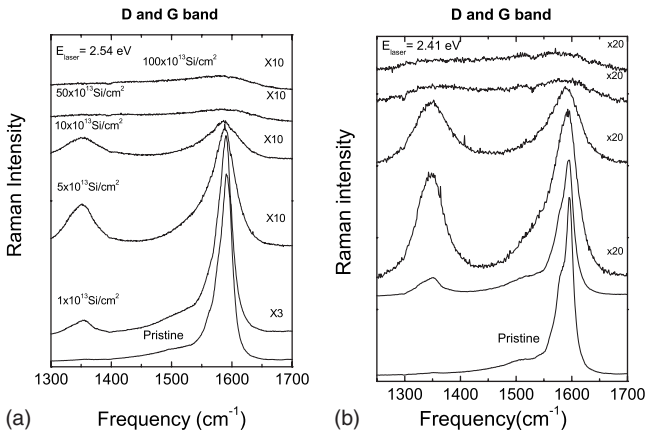

FIG. 3. *D*- and *G*-band Raman spectra of Si^+ ion bombarded DWNT samples for different excitation energies [(a) 2.54 eV and (b) 2.41 eV] and for different 170 keV Si^+ ion fluences. The same sample set was used for the data taken at the two laser energies.

that the inner and outer tube signals come from the same DWNT.

By examining the Kataura plot for SWNTs,[13] we can identify the outer or inner tube configurations that will be resonant for a given laser excitation energy and whether the tubes in resonance are semiconducting or metallic. We observe that for the $E_{\text{laser}}=2.54$ eV excitation, metallic inner tubes contribute to the RBM profile at 307, 289, and 268 cm^{-1} and semiconducting inner tubes contribute at 229 and 206 cm^{-1}. The excitation $E_{\text{laser}}=2.54$ eV is in resonance with the E_{11}^M transition for the metallic inner tube and with E_{33}^S for semiconducting inner tubes. The RBM peaks at 182, 168, and 145 cm^{-1} are associated with outer tubes for which $E_{\text{laser}}=2.54$ eV is in resonance with the E_{33}^S and E_{44}^S electronic transitions.

For $E_{\text{laser}}=2.41$ eV excitation, the spectra correspond to metallic inner tubes with ω_{RBM} at 318, 272, 264, and 253 cm^{-1} and semiconducting inner tubes at 329 and 214 cm^{-1}. The inner metallic tubes are in resonance with the E_{11}^M and the semiconducting inner tubes are in resonance with E_{22}^S. The strongest peak located near 272 cm^{-1} is associated with metallic tubes resonant with the $E_{11}^M(L)$ transitions (lower-energy branch associated with the trigonal warping effect). The outer tubes have RBM peaks at 175, 166, and 158 cm^{-1}, which are identified with E_{33}^S. The resonance Raman spectra of pristine DWNT samples, in the region of the *G* and *D* bands, are presented in Fig. 3 and described in Sec. III B 2 where comparisons are made to the ion-implanted tubes related to this pristine sample.

B. Si-implanted samples

1. RBM of inner vs outer tubes

The Si-implanted samples were irradiated using silicon ion doses varying from 1×10^{13} to 1×10^{15} Si^+/cm^2. Figure 2 shows the RBM spectra for the irradiated samples and the corresponding pristine sample for two different E_{laser} values. It can be observed that the intensity of the RBM modes rapidly decreases with increasing irradiation dose for both laser probing energies. For $E_{\text{laser}}=2.54$ eV, only two features appear to be present after a dose of 5×10^{13} Si^+/cm^2, the feature at around 229 cm^{-1} (semiconducting inner tube) and the feature at around 307 cm^{-1} (metallic inner tube), suggesting that the inner tubes are more resistant to radiation damage than the outer tubes. Indeed, molecular-dynamics calculations of ion-irradiated MWNTs are highly disordered by these levels of irradiation and the inner shells are less affected.[14] All the features appear to be completely quenched after a dose of 1×10^{14} Si^+/cm^2, thus indicating that both inner and outer tubes were severely damaged. Upon irradiation, small upshifts and downshifts of ω_{RBM} are also observed. For example, the RBM frequencies (obtained with $E_{\text{laser}}=2.41$ eV) for the sample irradiated with Si to a dose of 1×10^{13} ions/cm^2 were observed at 172, 210, 250, and 316 cm^{-1} which are softened as compared to the modes of the pristine sample (observed at 175, 214, 253, and 318 cm^{-1}, respectively). These changes could be due to nonuniform strain generated on the tube surface as a result of the ion bombardment. The defects introduced by the ion bombardment would modify the carbon bonds, thus affecting the lattice structure. Actually, it has been shown that ω_{RBM} is strongly dependent on the kind of deformation imposed on the tubes.[15]

2. G and D bands

Figure 3 shows the Raman spectra of pristine and Si-implanted DWNTs, in the region of the disorder-induced *D* band, and the *G* band. Regardless of the laser energy used for excitation, the *D* band is very weak in the Raman spectra of the pristine samples, indicating that the samples are of high crystalline quality. The *G*-band profiles obtained at $E_{\text{laser}}=2.41$ eV and $E_{\text{laser}}=2.54$ eV show a long tail toward low wave number, which is typical of a Breit-Wigner-Fano line shape. This line shape, in carbon nanotubes, comes from the resonant metallic inner tubes.[16] For the sample irradiated with a fluence of 1×10^{13} Si^+/cm^2, we observed an overall decrease (by a factor of 3) in the intensity of the spectrum

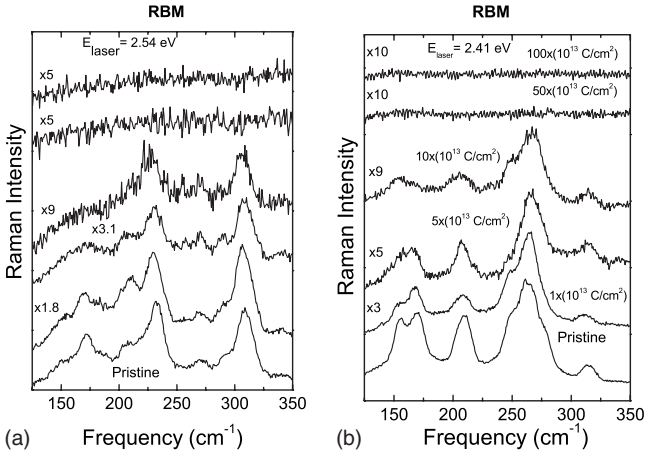

FIG. 4. RBM Raman spectra of 100 keV C^+ bombarded DWNT samples, for different laser excitation energies [(a) 2.54 eV and (b) 2.41 eV] and for different fluence levels. The same sample set was used for the data taken at the two laser energies.

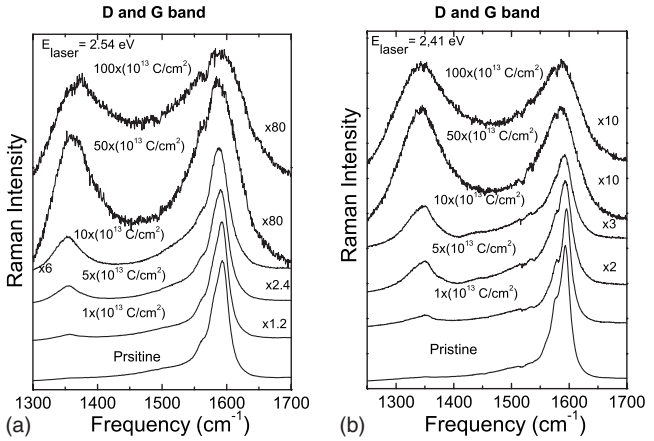

FIG. 5. *D*- and *G*-band Raman spectra of 100 keV C^+ bombarded DWNT samples for different excitation energies. (a) 2.54 eV and (b) 2.41 eV. The same sample set was used for the data taken at the two laser energies.

and the appearance of a significant *D* band, showing that structural disorder had been introduced into the nanotubes walls by the Si ion bombardment. For Si ion fluences increasing from 1×10^{13} to 1×10^{14} ions/cm^2, a gradual decrease in intensity of the *G* band and a concomitant increase in intensity of the *D* band, along with the broadening of both bands, were observed, indicating the increasingly higher degree of disorder introduced in the nanotubes. For fluences $\geq5\times10^{14}$ ions/cm^2, almost no spectral features could be observed in the Raman spectra, indicating that the samples were highly disordered.

The *G*-band feature observed in samples irradiated with a Si dose of 10×10^{13} ions/cm^2 is typical of carbon nanotubes, although the resonance Raman spectra for the RBM modes were not obtained, indicating that disorder affects the totally symmetric radial vibrational modes more strongly. Furthermore, the ion bombardment could induce bridges between the tubes which damp the radial atomic motions much more that the in-plane vibrations such as those that give rise to the *G* band. The *G*-band mode requires only a short neighbor interaction, while the RBM displacements are extended over the whole nanotube cylinder, which explains the stronger suppression of the RBM feature relative to the *G* band.

C. Carbon implantation

1. RBM bands

Figures 4(a) and 4(b) show the RBM Raman spectra for DWNTs, implanted with 100 keV C ions, using doses varying from 1×10^{13} to 1×10^{15} C/cm^2 and measured using E_{laser}=2.54 eV and E_{laser}=2.41 eV, respectively. The RBM spectral features decrease in intensity with increasing dose, but are clearly distinguishable upon implantation with 1×10^{14} C/cm^2 and disappear, somewhat suddenly, after implantation with 5×10^{14} C/cm^2. A comparison between Figs. 4 and 2 shows that the RBM bands for C ion-implanted samples remain observable for larger fluences than the corresponding Si implants.

2. G and D bands

Figure 5 shows the Raman spectra of pristine and C-implanted DWNTs, in the region of the disorder-induced *D* band, and the *G* band. Again, a gradual decrease in intensity of the *G* band and concomitant increase in intensity of the *D* band, along with the broadening of both bands, are observed upon irradiation with increasing C^+ ion dose. However, for C implantation, the *D* and *G* bands can be clearly distinguished, even for the largest fluence used, i.e., 1×10^{15} C/cm^2. Also, as observed in the case of Si implantation, the *D* and *G* bands are still present for carbon implantation doses at which the RBM modes are completely quenched.

IV. DISCUSSION

We have employed resonance Raman scattering spectroscopy to monitor the implantation of Si and C ions into DWNTs. Characteristic Raman spectral features of carbon nanotubes, such as the RBM, *G*, and *D* bands, have been seen to change in intensity, shape, and position (frequency) upon ion irradiation. We now analyze these changes in order to infer the changes induced by the ion bombardment to the crystalline structure and to the physical properties of the nanotubes.

A. Comparison between Si and C implanted samples

The penetration depth and width of the disordered region created by 170 keV Si ions or 100 keV C ions in carbon contained in DWNTs are not very different. A stopping and range of ions in matter (SRIM) simulation[17] shows that 170 keV Si ions and 100 keV C ions have approximated projected ranges of 400 ± 37 and 470 ± 37 nm, respectively, based on DWNTs with a density of 1.0 g/cm^3, and in both cases, the implantation-induced disorder extends from the surface to a depth of about 400–500 nm. However, the total number of lattice displacements (induced by the primary ion and the knocked-on C atoms), produced by a 170 keV Si^+

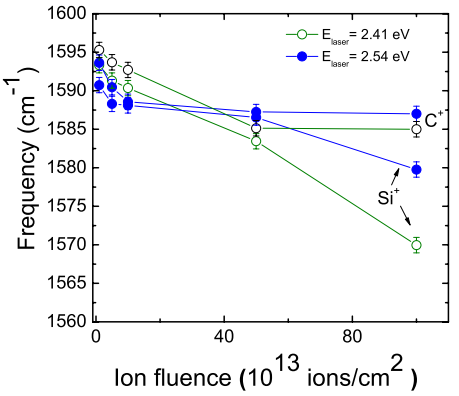

FIG. 6. (Color online) *G*-band Raman frequencies as a function of fluence for 170 keV Si^+ and 100 keV C^+ bombarded DWNT samples for different laser excitation energies. (a) 2.54 eV and (b) 2.41 eV.

ion, is about 3 times larger than the number produced by a 100 keV C^+ ion. Assuming these implantation parameters maintain similar relationships (Si vs C) in the case of the DWNT bucky paper samples used in the present study, it would be expected that the Si^+ implantation will create much more lattice disorder than the C^+ implantation for a similar dose. Indeed, this is the case, as shown by our experimental data. The RBM lines in the Raman spectra of DWNTs could still be distinguished after C^+ implantation with a dose of 1×10^{14} ions/cm^2, while for Si^+ implantation, the bands were completely attenuated after irradiation with the same dose. In addition, both the *G* and *D* bands of DWNTs implanted with 100 keV C^+, to a dose of 1×10^{15} ions/cm^2, were clearly visible, while for 170 keV Si^+ implanted samples, these spectral features were completely quenched for a fluence of 5×10^{14} ions/cm^2.

B. Evolution of lattice disorder

In Fig. 6, we show the G^+ (the *G* band in nanotubes has two most intense features which are labeled in order of increasing frequency as G^- and G^+) frequency dependence (measured with two laser lines) on fluence for both the Si^+ and C^+ bombarded samples. For the C^+ ion-bombarded samples, the G^+-band frequency softens as the ion fluence increases and it saturates around 1586 cm^{-1} which is typical of disordered carbon materials. In the case of the Si-implanted samples, the softening is larger and the saturation frequency for the largest ion dose is about 1570 cm^{-1}. This result can be understood by the model suggested by Ferrari and Robertson.[18] When defects are progressively introduced into the nanotube walls (on route to amorphization), these defects lead to the softening of phonon modes, particularly the softening of the *G* band. The results of Fig. 6 show that the sample is fully transformed into sp^2 amorphous carbon when the *G*-band frequency reaches 1575 cm^{-1}. It is important to note that for DWNTs exposed to high ion fluences, the *G* band develops an asymmetrical tail toward low frequencies, which indicates the formation of a Breit-Wigner-Fano line shape. This indicates the presence of some sp^3 in the amorphous carbon matrix.[19] For both the C^+ and Si^+ bombarded samples, the saturation frequency is different and this might be attributed to the different structural properties of the irradiated system particularly as the ion fluence becomes large. In the case of the Si^+ bombarded samples, the Raman spectra are typical of completely amorphous carbon, where the *D* and *G* band peaks are very broad and the features identified with nanotubes are no longer resolved. This regime is not reached for the fluence levels used for the C^+ irradiated samples, where we can see that the *D* band peak which becomes increasingly strong and broadened, it nevertheless appears well resolved without overlapping very much with the *G* band. The *D*-band and *G*-band profiles in the high-fluence limit in Fig. 5 look like that coming from a glassy carbon material.[20] The DWNTs in a bundled sample formed by ropes of tubes may under intermediate ranges of ion fluence generate disordered tubes with some confluence of different bundles, leading the sample to have a tangled morphology looking like a glassy carbon material.

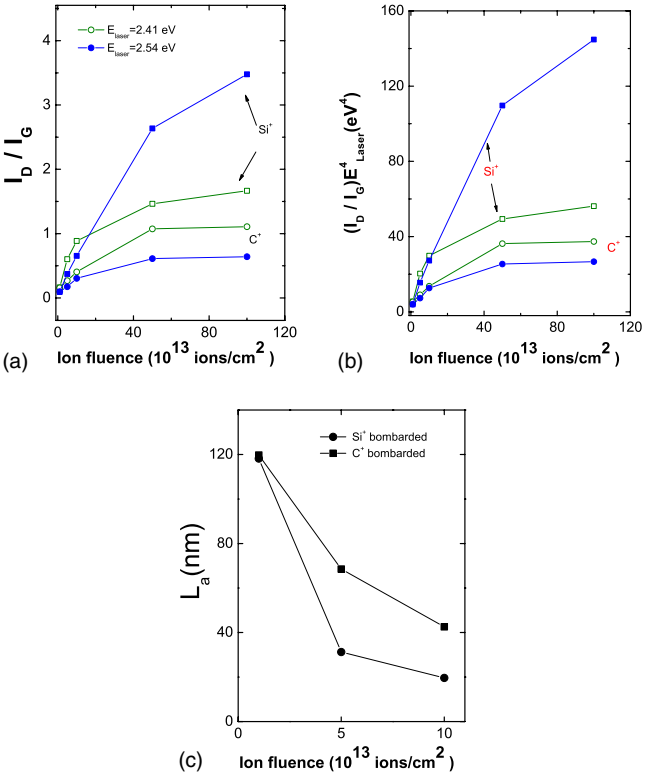

FIG. 7. (Color online) Plots of the dependence on ion fluence of the (a) I_D/I_G and (b) the normalized $(I_D/I_G)E^4_{\text{laser}}$ intensity ratio for Si^+ and C^+ bombarded DWNT samples as a function of ion fluences and for different excitation energies. In (c), we plot the characteristic length L_a for Si^+ and C^+ bombarded DWNT samples as obtained from the *D*- to *G*-band intensity ratio using the model of Cançado *et al.* (Ref. 24).

The *D* to *G* band intensity ratio (I_D/I_G) has been used as a parameter for characterizing the degree of disorder in sp^2 carbon networks, as well as for estimating the planar crystallite size L_a for sp^2-based carbon materials.[21] In Fig. 7(a), we show the plot of I_D/I_G as a function of C^+ and Si^+ ion bombardment doses for different laser lines. We can see that the I_D/I_G parameter increases as the dose increases, thus confirming the increasing density of defects in the DWNT

samples with increasing ion fluence. It is also clear that the I_D/I_G parameter depends strongly on the ion species used for the bombardment, as well as on the laser excitation energy. An empirical equation for correlating the I_D/I_G ratio with the crystallite size L_a was first proposed by Tuinstra *et al.*[21] and Knight *et al.*[22] but this equation did not take into account the laser energy dependence which was later discussed by Mernagh *et al.*[23] Recently, a generalized relation which considers both the laser energy dependence and the effect of defect production on I_D/I_G was proposed by Cançado and co-workers.[24] In their work, the crystallite size (in units of nm) together with the laser energy (in units of eV) is correlated by the following equation $L_a=(560/E_{\text{laser}}^4)\ (I_D/I_G)^{-1}$. Although the model was developed for graphite, it should apply to some extent for other sp^2-based materials such as carbon nanotubes.

In order to separate the contributions of laser excitation energy from the dose and the ion species, we normalized the I_D/I_G curves from Fig. 7(a) by E_{laser}^4 in accordance with the model of Cançado *et al.* [Fig. 7(b)]. After carrying out this normalization, we can see that the curves for a given ion-implanted sample show a unique curve only for ion doses up to 2×10^{14} ions/cm^2. Therefore, we can use Cançado's empirical equation for estimating the characteristic length L_a in this range for the bombarded DWNTs. Here, the L_a should be interpreted as a characteristic distance between the defects introduced by the ion beam into the carbon nanotube lattice. The L_a values are shown in Fig. 7(c). Here, we can see that this characteristic length dependence on ion fluence is stronger for Si^+ bombardment as compared to C^+, but both values show a tendency toward saturation. It has been demonstrated in the literature that carbon nanotubes when irradiated with electrons exhibit pronounced healing effects.[25] It is possible that the same healing mechanism is operational in the case of ion bombardment being more efficient in the case of the less damaging carbon irradiation (when compared to silicon irradiation).

The minimum crystallite size used by Cançado *et al.* for obtaining his empirical equation was 20 nm. In our bombarded samples, the lowest characteristic length determined from the range of L_a where the I_D/I_G ratio follows the E_{laser}^4 dependence also was about 20 nm [see Fig. 7(b)]. For doses larger than 40×10^{13} ions/cm^2, the equation does not exhibit the E_{laser}^4 dependence anymore and this is attributed to the very large density of defects which would translate into a very small crystal size. In this limit, the carbon lattice is likely to lose its sp^2-like character, thus forming amorphous carbon and carbon clusters with a reasonable amount of sp^3-like carbon. It seems that for Si-bombarded samples, the fraction of amorphous carbon and sp^3-like carbon is higher that for C-bombarded samples. This argument is based on the fact that the Raman cross section for sp^3 carbons is much lower than that for sp^2 carbon. Amorphous carbon nanowires were obtained in MWNTs by high doses (10^{15}–10^{17} ions/cm^2) from a 40 keV Si^+ ion beam.[26] The amorphous carbon nanowire is completely formed for fluences of 10^{17} ions/cm^2. The lower fluence 10^{15} ions/cm^2 only makes the MWNT layers very disordered, which indicates a higher stability against damage by the ion beam than DWNTs owing to the considerably larger number of layers in MWNTs.

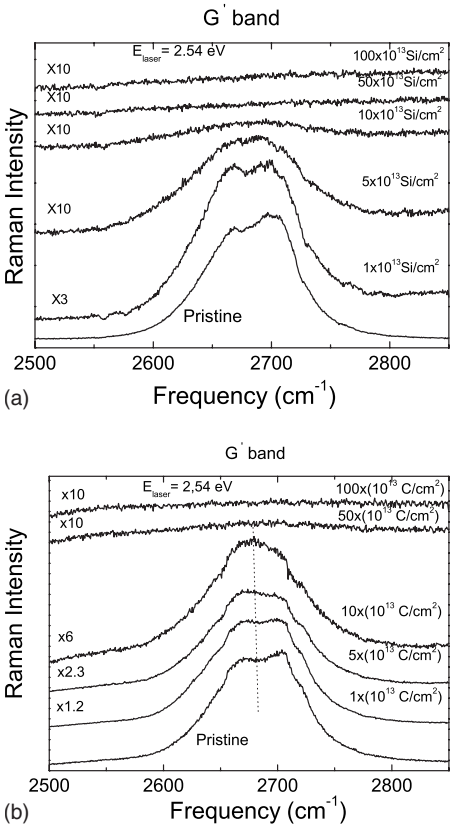

FIG. 8. G'-band Raman spectra of (a) 170 keV Si^+ and (b) 100 keV C^+ bombarded DWNT samples for 2.54 eV laser excitation energy.

Finally, the behavior of the I_D/I_G ratio as a function of ion fluence rules out the possibility of bombardment-induced nanographite because in this regime it is expected that the I_D/I_G ratio would exhibit an L_a^2 dependence following the Tuinstra model.[21] This dependence would imply a monotonic decrease in intensity of the curves shown in Fig. 7, instead of a saturation point, thus pointing out that the ion bombardment is not leading the samples to form nanocrystalline graphite.

Finally, in Figs. 8(a) and 8(b), we show the second-order G' band measured with $E_{\text{laser}}=2.54$ eV energy for DWNTs bombarded with Si^+ and C^+ ions, respectively. We can observe that the G' mode is completely quenched for fluences of 10×10^{13} ions/cm^2 in the case of the Si-bombarded samples and at 50×10^{13} ions/cm^2 for C-bombarded samples. Furthermore, the relative intensity of the lower frequency peak with respect to the higher frequency peak increases as the ion fluence increases. This is consistent with the observations in the RBM Raman data that point out that the inner tubes are the last ones to be affected by the ion beam, since the lower frequency peaks in the G' band of the DWNTs have contributions from the inner tubes[27] and they disappear first as the ion fluence increases (see Fig. 9). The disappearance of the G' band indicates the onset of the amorphous stage in the samples.

V. LASER ANNEALING OF THE IRRADIATED SAMPLES

In order to get further information on how the irradiation affects the DWNT structure, we have performed thermal an-

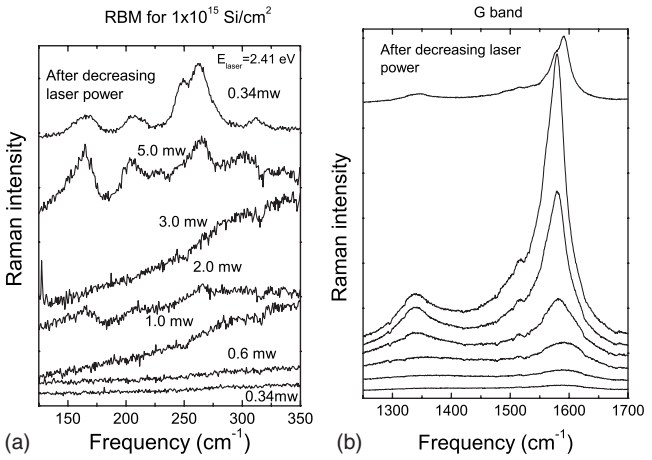

FIG. 9. (a) RBM and (b) *G*-band Raman spectra for a Si^+ irradiated sample initially exposed to 1×10^{15} ions/cm^2 for various laser power levels. The laser excitation energy was 2.41 eV.

nealing experiments on the irradiated samples. The thermal annealing consisted in increasing the power of the probing laser and exposing the sample for about 1 min prior to performing the Raman measurements using the same laser power level for another 5 min. This process provides thermal energy for the annealing of defects introduced by the ion implantation while simultaneously measuring the Raman spectra. In Fig. 9, we show data obtained for a sample with a higher degree of disorder, i.e., Si^+ irradiated DWNT samples with a fluence of 1×10^{15} ions/cm^2. We can clearly see in Fig. 9 that as the laser power is increased, the *G*-band signal gains intensity and at a certain laser power density (labeled 5.0 mW), the spectra look like the profile coming from the nonirradiated nanotubes with an enhanced *D* band. A similar effect is observed in the RBM, but here the modes clearly appear only for the highest laser power density used. After reaching the highest laser power level, we measured the same sample using the initial laser power level (0.34 mW) for which the spectrum is shown in the top trace of Fig. 9. Here we can observe that the RBM and *G* band are similar to the pristine signal (see Fig. 1), although the signal is very weak. This phenomenon was also observed and found to be more pronounced for other samples irradiated with lower fluences. These findings indicate that laser beam annealing can produce partial recovery of the defective nanotubes. By comparing the relative intensity of the RBM for the inner and outer tubes in these annealed samples to the pristine samples, it seems that the inner tubes are more reconstructed than the outer tubes. Since the inner tubes are less affected by the irradiation than the outer tubes, it is expected that an appropriate combination of implantation and annealing parameters could be used to modify the outer tubes while at same time preserving the properties of the inner tubes.

DWNTs vs SWNTs

The G'-band mode is well known to be extremely sensitive to stress and strain in the lattice.[28,29] For electron-irradiated SWNTs, a frequency upshift was observed in the G' band, indicating a compressive strain in the lattice upon irradiation but no such upshift was observed for C ion implantation.[8] The G' band for 4 MeV Ne-bombarded SWNTs did not show an upshift indicating that the amount of strain transferred to the lattice was quite small.[2] Although Si and C atoms have different masses, we did not observe any upshift in the G' band frequencies upon Si^+ and C^+ implantation, thus indicating that the ion implantation performed here did not introduce a detectable amount of strain into the carbon lattice.

VI. CONCLUSIONS

In summary, we have studied the effects of Si^+ and C^+ ion bombardment on the vibrational and structural properties of double wall carbon nanotubes. Resonance Raman spectroscopy data indicate that the outer tubes of the DWNTs are more affected by the ion bombardment than the inner tubes. As the ion-beam fluence increases, the tubes get disordered as indicated by the increase in the *D* to *G* band intensity ratio (I_D/I_G) and this effect is much stronger for implantation with Si^+ as compared to C^+. The lattice disorder introduced by the ion irradiation can be removed by laser annealing of the samples. These observations suggest that it might be possible to modify nanotube properties in a tailored fashion by employing combined implantation and annealing processes. Furthermore, it is hoped that this initial survey of ion-implanted DWNTs will stimulate theoretical studies of ion bombardment in DWNTs because DWNTs provide a model system for gaining a better understanding of defect formation in carbon nanotubes as well as in other systems such as bilayer graphene.

ACKNOWLEDGMENTS

Financial support from CNPq, FUNCAP, CAPES, and FAPERGS is gratefully acknowledged. M.S.D. acknowledges the support from NSF Grant No. 07-01497. A.G.S.F. acknowledges the support from CNPq (Grants No. 306335/2007-7, No. 503956/2007-4, and No. 577489/2008-9). The authors acknowledge financial support from Rede Nacional de Pesquisa em Nanotubos de Carbono. The NSF-CNPq (Grant No. 491083/2005-0) for joint collaboration is also acknowledged. M.E. acknowledges the support from the CLUSTER (second stage) and MEXT grants (No. 19002007). G.D.S. acknowledges the support from CNPq (480364/2008-7).

*agsf@fisica.ufc.br

[1] M. Endo, M. S. Strano, and P. M. Ajayan, in *Carbon Nanotubes*, edited by A. Jorio, M. S. Dresselhaus, and G. Dresselhaus, Topics in Applied Physics Vol. 111 (Springer-Verlag, Berlin, 2008), pp. 13–61.
[2] A. R. Adhikari, M. Huang, H. Bakhru, R. Vajtai, C. Y. Ryu, and P. M. Ajayan, J. Appl. Phys. **100**, 064315 (2006).
[3] A. V. Krasheninnikov and F. Banhart, Nature Mater. **6**, 723 (2007).
[4] B. Q. Wei, J. Darcy-Gall, P. M. Ajayan, and G. Ramanath, Appl. Phys. Lett. **83**, 3581 (2003).
[5] M. Bockrath, W. Liang, D. Bozovic, J. H. Hafner, C. M. Lieber, M. Tinkham, and H. Park, Science **291**, 283 (2001).
[6] M. Terrones, H. Terrones, F. Banhart, J. C. Charlier, and P. M. Ajayan, Science **288**, 1226 (2000).
[7] A. V. Krasheninnikov, K. Nordlund, J. Keinonen, and F. Banhart, Phys. Rev. B **66**, 245403 (2002).
[8] S. Gupta and R. J. Patel, J. Raman Spectrosc. **38**, 188 (2007).
[9] S. K. Pregler, B.-W. Jeong, and S. B. Sinnott, Compos. Sci. Technol. **68**, 2049 (2008).
[10] A. G. Souza Filho, V. Meunier, M. Terrones, B. G. Sumpter, E. B. Barros, F. Villalpando-Páez, J. Mendes Filho, Y. A. Kim, H. Muramatsu, T. Hayashi, M. Endo, and M. S. Dresselhaus, Nano Lett. **7**, 2383 (2007).
[11] M. S. Dresselhaus, G. Dresselhaus, A. Jorio, A. G. Souza Filho, Ge. G. Samsonidze, and R. Saito, J. Nanosci. Nanotechnol. **3**, 19 (2003).
[12] M. Endo, T. Hayashi, H. Muramatsua, Y.-A. Kim, H. Terrones, M. Terrones, and M. S. Dresselhaus, Nano Lett. **4**, 1451 (2004).
[13] A. Jorio, C. Fantini, M. A. Pimenta, R. B. Capaz, Ge. G. Samsonidze, G. Dresselhaus, M. S. Dresselhaus, J. Jiang, N. Kobayashi, A. Grüneis, and R. Saito, Phys. Rev. B **71**, 075401 (2005).
[14] S. K. Pregler and S. B. Sinnott, Phys. Rev. B **73**, 224106 (2006).
[15] B. Gao, X. J. Duan, J. Zhang, T. J. Wu, H. B. Son, J. Kong, and Z. F. Liu, Nano Lett. **7**, 750 (2007).
[16] S. D. M. Brown, A. Jorio, P. Corio, M. S. Dresselhaus, G. Dresselhaus, R. Saito, and K. Kneipp, Phys. Rev. B **63**, 155414 (2001).
[17] J. F. Ziegler, Nucl. Instrum. Methods Phys. Res. B **219-220**, 1027 (2004).
[18] A. C. Ferrari and J. Robertson, Phys. Rev. B **61**, 14095 (2000).
[19] Y. Miyajima, S. J. Henley, G. Adamopoulos, V. Stolojan, E. Garcia-Caurel, B. Drévillon, J. M. Shannon, and S. R. P. Silva, J. Appl. Phys. **105**, 073521 (2009).
[20] M. S. Dresselhaus and R. Kalish, *Ion Implantation in Diamond, Graphite and Related Materials*, Springer Series in Materials Science Vol. 22 (Springer-Verlag, Berlin, 1992).
[21] F. Tuinstra and J. L. Koenig, J. Chem. Phys. **53**, 1126 (1970).
[22] D. S. Knight and W. B. White, J. Mater. Res. **4**, 385 (1989).
[23] T. P. Mernagh, R. P. Cooney, and R. A. Johnson, Carbon **22**, 39 (1984).
[24] L. G. Cançado, K. Takai, T. Enoki, M. Endo, Y. A. Kim, H. Mizusaki, A. Jorio, L. N. Coelho, R. Magalhaes-Paniago, and M. A. Pimenta, Appl. Phys. Lett. **88**, 163106 (2006).
[25] A. Kis, K. Jensen, S. Aloni, W. Mickelson, and A. Zettl, Phys. Rev. Lett. **97**, 025501 (2006).
[26] Z. Ni, Q. Li, J. Gong, D. Zhu, and Z. Zhu, Nucl. Instrum. Methods Phys. Res. B **260**, 542 (2007).
[27] E. B. Barros, H. B. Son, Ge. G. Samsonidze, A. G. Souza Filho, J. Mendes Filho, G. Dresselhaus, and M. S. Dresselhaus, Phys. Rev. B **76**, 035444 (2007).
[28] J. Sandler, M. S. P. Shaffer, A. H. Windle, M. P. Halsall, M. A. Montes-Moran, C. A. Cooper, and R. J. Young, Phys. Rev. B **67**, 035417 (2003).
[29] O. Lourie and H. D. Wagner, J. Mater. Res. **13**, 2418 (1998).